



THE UNIVERSITY *of* EDINBURGH

Edinburgh Research Explorer

## Linkages between tropical Pacific seasonal, interannual, and orbital variability during the Holocene

**Citation for published version:**

Emile-Geay, J, Cobb, KM, Carre, M, Braconnot, P, Leloup, J, Zhou, Y, Harrison, SP, Correge, T, McGregor, HV, Collins, M, Driscoll, R, Elliot, M, Schneider, B & Tudhope, A 2016, 'Linkages between tropical Pacific seasonal, interannual, and orbital variability during the Holocene', *Nature Geoscience*, vol. 9, pp. 168-173. <https://doi.org/10.1038/ngeo2608>

**Digital Object Identifier (DOI):**

[10.1038/ngeo2608](https://doi.org/10.1038/ngeo2608)

**Link:**

[Link to publication record in Edinburgh Research Explorer](#)

**Document Version:**

Peer reviewed version

**Published In:**

Nature Geoscience

**General rights**

Copyright for the publications made accessible via the Edinburgh Research Explorer is retained by the author(s) and / or other copyright owners and it is a condition of accessing these publications that users recognise and abide by the legal requirements associated with these rights.

**Take down policy**

The University of Edinburgh has made every reasonable effort to ensure that Edinburgh Research Explorer content complies with UK legislation. If you believe that the public display of this file breaches copyright please contact [openaccess@ed.ac.uk](mailto:openaccess@ed.ac.uk) providing details, and we will remove access to the work immediately and investigate your claim.



# 1 **Linkages between tropical Pacific seasonal, interannual,** 2 **and orbital variability during the Holocene**

3 J. Emile-Geay<sup>1\*</sup>, K.M. Cobb<sup>2</sup>, M. Carré<sup>3</sup>, P. Braconnot<sup>4</sup>, J. Leloup<sup>5</sup>, Y. Zhou<sup>1</sup>,

4 S.P. Harrison<sup>6</sup>, T. Corrège<sup>7</sup>, H.V. McGregor<sup>8</sup>, M. Collins<sup>9</sup>, R. Driscoll<sup>10</sup>, M. Elliot<sup>11</sup>,

5 B. Schneider<sup>12</sup>, A. Tudhope<sup>10</sup>

6 <sup>1</sup>*Department of Earth Sciences, University of Southern California, Los Angeles, CA 90089, USA*

7 <sup>2</sup>*School of Earth and Atmospheric Sciences, Georgia Institute of Technology, Atlanta, GA 30332,*

8 *USA*

9 <sup>3</sup>*Institut des Sciences de l'Evolution, Université de Montpellier, CNRS, IRD, EPHE, Montpellier*

10 *34095, France*

11 <sup>4</sup>*IPSL/LSCE, unité mixte CEA-CNRS-UVSQ, Gif sur Yvette 91191, France*

12 <sup>5</sup>*Sorbonne Universités, UPMC Univ. Paris 6, LOCEAN/IPSL, UMR 7159, CNRS-IRD-MNHN,*

13 *Paris, France*

14 <sup>6</sup>*Centre for Past Climate Change and School of Archaeology, Geography and Environmental Sci-*

15 *ences (SAGES) University of Reading, Whiteknights, Reading, RG6 6AB, UK*

16 <sup>7</sup>*UMR 5805 EPOC, Université de Bordeaux, Pessac, France*

17 <sup>8</sup>*School of Earth and Environmental Sciences, University of Wollongong, Wollongong, NSW*

18 *2522, Australia*

19 <sup>9</sup>*College of Engineering, Mathematics and Physical Sciences, University of Exeter, Laver Build-*

20 *ing, North Park Road, Exeter, EX4 4QE, UK*

21 <sup>10</sup>*University of Edinburgh, School of GeoSciences, James Hutton Road, Edinburgh EH9 3FE, UK*

22 <sup>11</sup>*Paleoclimats Paleoenvironnements Bioindicateurs, Université de Nantes, LPGNantes, 2 rue de*  
23 *la Houssinière, Nantes 44300, France*

24 <sup>12</sup>*Institut für Geowissenschaften, Universität Kiel, D-24118 Kiel, Germany*

25 **The response of the El Niño/ Southern Oscillation (ENSO) to external forcing is a central**  
26 **issue in climate science. It is unclear how ENSO responds to natural forcing, particularly**  
27 **orbitally-induced changes in the amplitude of the seasonal cycle. Here we reconstruct sea-**  
28 **sonal and interannual variability using a network of high-resolution marine records from**  
29 **the tropical Pacific Ocean spanning discrete intervals of the Holocene. We then compare**  
30 **our reconstructed ENSO activity to that simulated by nine climate models. The records**  
31 **display several intervals of reduced ENSO variance, notably a 2/3 reduction between 5,000**  
32 **and 3,000 years ago. The reconstructed changes are not in phase with equatorial insolation,**  
33 **nor is their amplitude or timing accurately captured by the models. Moreover, the models**  
34 **do not predict the mid-Holocene increase in seasonality evident in the observations. While**  
35 **the simulations suggest an inverse relationship between the amplitude of the seasonal cycle**  
36 **and ENSO-related variance in sea surface temperatures, the observations do not. We there-**  
37 **fore conclude that tropical Pacific climate is highly variable and subject to millennial-scale**  
38 **quiescent periods. Such periods harbor a complex link, if any, to orbital forcing, and are**  
39 **inadequately simulated by the current generation of climate models, highlighting a major**  
40 **gap in our understanding of a climate system of global importance.**

41 ENSO, the oscillatory instability of the tropical Pacific ocean–atmosphere system, is the  
42 leading pattern of global interannual variability, with important physical, ecological, and human

43 impacts<sup>1</sup>. Yet, predicting its long-term behavior in the face of continued anthropogenic forcing  
44 has proven elusive<sup>2</sup>. While the predictive skill of climate models at interannual timescales can be  
45 tested using instrumental observations, such records are too short to evaluate the fidelity of model-  
46 simulated tropical Pacific variability on adaptation-relevant timescales. This motivates the use  
47 of paleoclimate observations, which cover a much longer time span and predate the instrumental  
48 observations used to develop and tune climate models, hence providing an out-of-sample test of  
49 their predictive ability<sup>3</sup>.

50 The mid-Holocene (MH, ca 6,500 yrs before present; 6.5 kyBP) represents a key target for  
51 evaluating the simulated response of ENSO to external forcing. While ice volume and greenhouse  
52 gas concentrations were essentially similar to today, the latitudinal and seasonal distribution of  
53 incoming solar radiation (insolation) was markedly different as a result of precession<sup>4</sup>: seasonal  
54 contrast was amplified in the northern hemisphere and reduced in the southern hemisphere. Thus,  
55 the mid-Holocene provides an opportunity to explore the link between changes in the seasonal  
56 cycle, meridional asymmetry in the equatorial zone, and ENSO behavior. Several circum-Pacific  
57 paleoclimate records have been interpreted as implying a marked reduction in ENSO activity dur-  
58 ing the MH<sup>5-7</sup>, a reduction simulated by models of various complexity<sup>8-13</sup>. Furthermore, this  
59 reduction has been dynamically linked either to changes in the linear stability of ENSO<sup>9</sup>, or to an  
60 insolation-driven increase in the amplitude of the annual cycle in near-equatorial SST (hereafter,  
61 AC)<sup>9,10,12</sup>, in line with evidence for a negative correlation between ENSO and the AC documented  
62 in instrumental observations<sup>14</sup> and modeling studies of current and past climate states<sup>8,15-19</sup>.

63 Several mechanisms have been proposed to account for the seasonal cycle influence on  
64 ENSO: frequency locking<sup>15,20</sup>; nonlinear resonance between annual and internal modes<sup>21,22</sup>, and  
65 combination tones of ENSO and the AC<sup>23</sup>. We note, however, that the inverse link between ENSO  
66 variance and AC amplitude is not universal amongst models<sup>4,10</sup> nor in the various proposed mech-  
67 anisms. While some seasonally-resolved paleoclimate records suggest a strong dynamical link  
68 between precessional forcing and ENSO activity<sup>24</sup>, reconstructions of central and eastern Pacific  
69 ENSO variance do not<sup>25,26</sup>. A synthesis of the available observations and simulations of ENSO  
70 and the annual cycle is timely, and would help constrain ENSO sensitivity to external forcing.

71 Here we synthesize high-resolution, well-dated paleoclimate records from across the trop-  
72 ical Pacific spanning the Holocene (see Extended Methods). We compare these observations  
73 to an ensemble of nine state-of-the-art global climate models (GCMs) from the Paleoclimate  
74 Modeling Intercomparison Project (PMIP3<sup>27</sup>), which include simulations of pre-industrial (*piCon-*  
75 *trol*) as well as industrial (*historical*) and MH (*midHolocene*) climate (Supplementary Table S2).  
76 This dataset constitutes the most comprehensive collection of oxygen isotope measurements on  
77 Holocene corals<sup>5,6,24,25,28–34</sup> and mollusks<sup>26,35–37</sup> to date from the tropical Pacific (Figure 1, Sup-  
78 plementary Table S1, Supplementary Figures S1-S6). Such marine carbonates record the isotopic  
79 composition of oxygen ( $\delta^{18}\text{O}$ ), which reflects changes in sea-surface temperature (SST, Supple-  
80 mentary Figure S10a) as well as the  $\delta^{18}\text{O}$  of seawater (the latter linearly related to sea-surface  
81 salinity (SSS, Supplementary Figure S10b). The isotopic signal is generally dominated by the  
82 thermal component, except in the far western Pacific (Supplementary Figure S11). All records  
83 have annual or finer resolution and collectively cover  $\sim 2000$  out of the past 10,000 years (Sup-

84 plementary Table S1 and Figure S1). There are three clusters of sites in the western (WP: Papua  
85 New Guinea, New Caledonia, Vanuatu, Surprise Atoll), central (CP: the Line Islands of Palmyra,  
86 Fanning and Christmas) and eastern (EP: Peruvian coast) tropical Pacific.

### 87 **Seasonal and interannual variability over the Holocene**

88 The seasonal and interannual components of the tropical Pacific records display much irregularity  
89 in interannual (2–7y) variance – a measure of ENSO activity – as well as in AC amplitude. To en-  
90 able comparisons between different records and sites, we show the ratio between fossil and modern  
91 (twentieth century) values of interannual variance and AC amplitude (Figure 2), with uncertainties  
92 estimated via the block bootstrap (Extended Methods). Most records of ENSO variance plot below  
93 unity, implying that twentieth century ENSO was unusually active<sup>25,38</sup>. Those fossil samples dis-  
94 playing higher-than-modern ENSO variance have large uncertainties compatible with no change.  
95 Such uncertainties are usually the consequence of short fossil and/or modern sequences.

96 Despite appreciable differences between ENSO reconstructions from the three regions, some  
97 consistent patterns do emerge. In the western Pacific (Figure 2, top), the records show a significant  
98 decrease in ENSO variance during the early and mid-Holocene<sup>5,6,29,36</sup>; there are only a few records  
99 from the 6-2 kyBP interval but these also show reduced ENSO variance. Low ENSO variance is  
100 present throughout the past 7ky in the CP (Figure 2, center), with the most consistent signal cor-  
101 responding to a 64% reduction occurring between 3-5 kyBP (Table 1) and a trend from extremely  
102 low variance to the present state from 2 kyBP onwards<sup>24,25</sup>. Records from the EP show ENSO

103 variance either similar to or lower than today, with the deepest reduction around 4.6 kyBP (Figure  
104 2, bottom)<sup>26</sup>. Thus, our data set suggests that the mid-Holocene reduction in ENSO variance iden-  
105 tified in previous studies<sup>5-7,32</sup> is not an exceptional event, but rather that ENSO may have been less  
106 active than at present for much of the Holocene.

107 Reconstructions of the AC amplitude display little coherence through time. Records from the  
108 western Pacific show AC amplitudes similar to present before 7 kyBP. However, records from the  
109 interval 7-4 kyBP unequivocally display a reduced AC amplitude, while after 3 kyBP the records  
110 show a return to AC amplitudes similar to the present day. In contrast, records from the CP show  
111 considerable temporal structure in AC amplitude, although many of the individual records have  
112 high levels of uncertainty. In the eastern Pacific, the records show slightly reduced AC amplitude  
113 throughout the past 10 ky, except for a period with amplitude similar to the present day at 3 kyBP.

#### 114 **Comparisons with simulated tropical Pacific climates**

115 We now use this dataset to constrain the behavior of PMIP3 models. Although there are com-  
116 paratively few records from precisely 6.5 kyBP, we assume that the changes recorded during the  
117 window between ca 7.5 and 5.5 kyBP are representative of the mid-Holocene and provide an indi-  
118 cation of the average change to be expected in the MH simulations. In order to make quantitative  
119 model-data comparisons, we translate model output into oxygen isotope ratios using a forward  
120 modeling approach<sup>39,40</sup>, in which the  $\delta^{18}\text{O}$  of biocarbonates is parameterized as a function of SSS  
121 and SST (Extended Methods). This approximates the isotopic variations that would have been

122 recorded by the coral or mollusk in response to the simulated changes in climate produced by each  
123 climate model, which can then be directly compared to the observed variations at a site (Supple-  
124 mentary Figures S10, S11). The forward model is a simplified representation of the incorporation  
125 of  $^{18}\text{O}$  by mollusk and coral systems, in particular because it represents the relationship between  
126 seawater  $^{18}\text{O}$  and SSS as time-invariant. However, it has been shown to reproduce the first-order  
127 basin-scale variability contained in modern corals from across the tropical Pacific<sup>39</sup>. Thus, this  
128 simple model provides a way of bridging GCMs and paleo observations.

129 Most of our records are comparatively short: the average record length is around 50 years  
130 (Supplementary Figure S1b) and very few are longer than 100 years. As ENSO variability is  
131 non-stationary, quantifying ENSO variance over such short windows leads to a wide range of  
132 estimates<sup>41,42</sup>. Random sampling of multi-century model simulations under stationary boundary  
133 conditions shows that ENSO variance estimates on 50-year windows may vary by up to  $\pm 50\%$   
134 from sampling alone (Supplementary Figure S13); these estimates converge as the observation  
135 window lengthens. Thus, the short length of most of the observations could make it difficult to  
136 discriminate between observed and simulated variability. Changes in the AC amplitude are much  
137 better constrained, though still sensitive to segment length (Supplementary Figures S12, S13).

138 For each model, we estimate the statistical distributions of modeled ENSO and AC amplitude  
139 for 50-year periods via the block bootstrap for both the *piControl* and *midHolocene* simulations  
140 (Supplementary Table S2) and compare these distributions to the values obtained from the *histor-*  
141 *ical* simulations (Supplementary Figures S14-22). The distributions of ENSO variance ratios are

142 broad and positively skewed, while those of AC amplitude are narrow and symmetric (Figure 2,  
143 colored curves). ENSO variance ratios are clustered around unity in the *piControl* experiments,  
144 and fall below unity in most of the *midHolocene* experiments. The *midHolocene* reduction is small  
145 and, given the width of the distributions, only marginally significant at the 5% level. Nonetheless,  
146 it is qualitatively consistent with results from an intermediate complexity model<sup>8</sup> as well as many  
147 other GCM simulations<sup>9-13</sup>, all of which show reduced ENSO variability during the mid-Holocene  
148 compared to the pre-industrial climate.

149 While the synthesis of existing paleo-ENSO data present a heterogeneous picture of ENSO  
150 variability through both space and time, there is evidence for a sustained reduction in ENSO vari-  
151 ability from 3-5 kyBP. This is especially true in the CP, where a deep reduction (64%) is accompa-  
152 nied by a relatively narrow 95% confidence interval (CI) of [28%, 84%] (Table 1). Reductions of  
153 similar magnitude are observed during the MH (5.5-7.5 kyBP) (66% in the center, 50% in the West,  
154 33% in the East), albeit with CIs so wide that they cannot exclude increases in ENSO variance (Ta-  
155 ble 1). Thus, a salient feature of this dataset is a robust, approximately two-thirds reduction in  
156 CP interannual variance, which appears to have persisted throughout much of the 3-5 kyBP in-  
157 terval. This persistent reduction bears little resemblance to the model simulations of reduced MH  
158 ENSO<sup>4,8</sup> followed by a gradual intensification to the present<sup>13</sup>, and happened at a time when boreal  
159 summer/winter precessional forcing was weaker than during the MH (Supplementary Figure S9).

160 Can PMIP3 GCMs simulate the magnitude of such reductions, and if so, under which con-  
161 ditions? We answer this question by computing the probability of observing ENSO variance re-

162 ductions of at least 64% on 50-year segments (Table 2). These probabilities are extremely low  
163 under pre-industrial conditions, ranging from 1 to 12%. Such occurrences are still rare under MH  
164 boundary conditions (probabilities ranging from 3 to 15%), though most (7 out of 9) of the models  
165 show an increased probability of ENSO reduction. Thus, while orbital forcing characteristic of  
166 the MH tends to drive simulated changes in ENSO variance in the right direction, the amplitude  
167 of simulated changes is too modest, and the response is not consistent among models. It is even  
168 harder to explain the larger, more sustained reductions that may have prevailed during the 3-5 kyBP  
169 period, but the short length of the simulations (Supplementary Table S2) precludes an assessment  
170 of this question.

171 The models all show a reduction in the median amplitude of the AC in the *midHolocene*  
172 simulations, for all three regions. The reduction is between 10% to 50% (depending on the model)  
173 but is relatively uniform across the basin (Figure 2, right). This uniformity contrasts strongly with  
174 the observed changes in the 7.5-5.5 kyBP window, where AC amplitude is decreased in the western  
175 Pacific but increased in the CP. However, the reduction in AC amplitude in the western Pacific is  
176  $\sim 50\%$  larger than in the simulations.

### 177 **Links between ENSO and the seasonal cycle amplitude**

178 We investigate the link between changes in ENSO variance and in AC amplitude by plotting the  
179 fossil to modern ratio of ENSO-band variance against the same ratio of AC amplitude, in both  
180 Holocene observations and PMIP3 simulations (Figure 3). Both axes are scaled by their uncer-

181 tainty to make an orthogonal regression possible (Extended Methods). The simulated relationship  
182 is significantly negative (Figure 3, bottom), in agreement with previous work<sup>17–20</sup>. This contrasts  
183 with the observations, which reveal a weak positive relationship between ENSO variance and AC  
184 amplitude (Figure 3, top). Moreover, the range of variations in AC amplitude is about 2-3 times  
185 larger in the observations than in the simulations (Supplementary Figure S23). Similar results  
186 emerge if only data from the CP are considered (Supplementary Figures S24–25), or if wavelet  
187 analysis is used to diagnose the relationship between energy in the annual and interannual bands<sup>19</sup>  
188 (Extended Methods, Supplementary Figure S26). If our interpretation of the data is correct, the  
189 mismatch between the observed and simulated relationship between ENSO variance and AC ampli-  
190 tude has important dynamical implications. The frequency entrainment hypothesis<sup>15,20</sup> states that  
191 a self-exciting oscillator will give up its independent mode of oscillation and acquire the frequency  
192 of the applied forcing (in this case, the AC in insolation). It has long been invoked to explain the  
193 inverse relationship between ENSO and the AC in coupled GCMs<sup>12,13,17,18</sup>. Our results confirm  
194 that this link is strong in PMIP3 models, but suggest that it is opposite to that found in observations  
195 over the Holocene.

196 In comparing the ENSO-AC relationship across models and data, it is important to note the  
197 limitations associated with using a sparse set of observations to constrain tropical Pacific dynam-  
198 ics. One possible explanation for the model-data mismatch in the ENSO-AC relationship is that  
199 uncertainties in AC amplitude estimates from corals are more uncertain than depicted by the boot-  
200 strap intervals, as documented by discrepancies of up to 30% in AC estimates from overlapping  
201 coral  $\delta^{18}\text{O}$  records from the central tropical Pacific (Supplementary Figure S12). The relationship

202 between  $\delta^{18}\text{O}$  and SSS is poorly constrained on subannual scales, and may vary across a given  
203 reef environment, further confounding estimates of AC amplitude changes from high-resolution  
204 archives. Results are, however, insensitive to the choice of ENSO metric as long as fossil/modern  
205 ratios are used (Supplementary Figure S27).

206 Changes in the spatial characteristics of ENSO represent another source of uncertainty, as  
207 different flavors of ENSO have different impacts on SST and SSS across the study domain. Canon-  
208 ical El Niño events involve temperature changes in the eastern Pacific (EP). However, many events  
209 peak in the CP<sup>43</sup>. Indeed, changes in the prevalence of ENSO flavors in the Holocene have been  
210 suggested by changes in the asymmetry of ENSO anomalies in the eastern Pacific<sup>26</sup> as well as  
211 analysis of PMIP3 *midHolocene* simulations<sup>12,44</sup>. Thus, some of the observed variations in ENSO  
212 intensity/frequency over the Holocene could reflect changes in the spatial pattern of ENSO and  
213 differences between individual records could reflect a dominance of one expression of ENSO over  
214 another<sup>26</sup>. However, an empirical ENSO model suggests that modern changes in the prevalence of  
215 ENSO flavors may arise internally<sup>45</sup>. Our dataset is too sparse to resolve spatial features of ENSO  
216 or the AC structure, but it is hoped that denser proxy networks will shed light on these questions  
217 in the future.

## 218 **Implications for ENSO dynamics**

219 It has been suggested that boreal fall insolation, which peaks at  $\sim 5$  kyBP (Supplementary Figure  
220 S8), modulates ENSO variability via air/sea coupling strength<sup>8</sup>. Our analyses reveal that changes in

221 ENSO variance and AC amplitude over the Holocene bear no simple relation to orbital forcing, ex-  
222 cluding a linear mechanism. It is possible that millennial-scale changes in ENSO variability arose  
223 either (1) internally, (2) as a non-linear response to orbital forcing, or (3) because of other factors,  
224 such as the presence of a remnant Laurentide ice sheet, which modulated the response to orbital  
225 forcing<sup>46</sup>. Our observations suggest persistent changes in ENSO variance and AC amplitude that  
226 fall well outside the range shown by both *piControl* and *midHolocene* PMIP3 simulations, partic-  
227 ularly during the 3-5 kyBP interval. The PMIP3 ensemble does not capture the potential range of  
228 ENSO variability over this interval, which should become a key target for climate models of vary-  
229 ing complexity to simulate and explain. One challenge in simulating such changes with GCMs is  
230 that computational requirements restrict simulations to 200-500yrs, on average. Additional long  
231 transient runs, both forced<sup>13</sup> and unforced<sup>41</sup>, would help distinguish endogenous from exogenous  
232 sources of ENSO variability. Furthermore, the simulated relationship between ENSO variance and  
233 AC amplitude is incompatible with observations. GCMs where an inverse relationship to AC am-  
234 plitude dominates the ENSO response to orbital forcing may therefore not be representative of the  
235 real world. Given that the mean state, AC and ENSO are so tightly connected<sup>16,47</sup>, the substantial  
236 climatological biases in CMIP5 models<sup>48</sup> are a logical suspect for this exaggerated relationship. Of  
237 particular relevance is the SST-shortwave feedback<sup>49</sup>, the asymmetric nature of which is not cap-  
238 tured by many state-of-the-art GCMs<sup>48</sup>. Even those GCMs that qualitatively simulate the feedback  
239 may do so via error compensation, so we speculate that large improvements in ENSO simulations  
240 would result from a correct representation of the underlying processes.

241 While precessional and greenhouse gas forcing are fundamentally different in character, our

242 work demonstrates the ability of high-resolution palaeoclimate records to provide fundamental  
243 constraints on tropical climate dynamics, as represented in models used to project twenty-first  
244 century climate trends. In that context, the fact that ENSO seemed relatively impervious to a large  
245 external forcing suggests that processes internal to the climate system could dominate external  
246 influences. Understanding internal processes of low-frequency ENSO modulation, and the extent  
247 to which they are captured by climate models, is therefore of utmost importance to improving  
248 climate projections.

## 249 **Extended Methods**

250 **Observational synthesis.** We compiled isotopic records obtained on coral or mollusks from 65  
251 sites in the Pacific (Table S1). The majority of the records have been published<sup>5,6,24–26,28–37</sup>, but  
252 some are published for the first time here (Supplementary Information). Most of the individual  
253 records are comparatively short (50 years or less, Supplementary Figure 1). The records sample  
254 2162 years out of the past 10,000 years (Supplementary Figure 1, Supplementary Table 1).

255 For analytical purposes, we group the individual sites into three separate regions:

256 **West** [120, 180, 20°S, 0°N], including Papua New Guinea and New Caledonia

257 **Center** [170°W, 120°W, 5°S, 5°N], corresponding to the NINO3.4 region (for which the SST average  
258 is a key ENSO indicator) and encompassing part of the Line Islands.

259 **East** [90°W, 80°W, 5°S, 5°N], corresponding to the NINO1+2 regions, a primary region to moni-

260 tor coastal warming.

261 Figure 1 shows that these three climatically-meaningful regions encompass the majority of the  
262 sites. Note that the sites of ref 26, while formally outside the NINO1+2 region (eastern box) are  
263 interpreted as reflecting NINO1+2 SST<sup>35</sup>.

264 **Analysis of observations.** Changes in ENSO variance were quantified by computing the ratio of  
265 fossil to modern variance in the 2-7y band. In continuous records, the latter was isolated via a  
266 (Morlet) wavelet filter (Supplementary Figure 7), while for peruvian mollusks we used the ratio of  
267 fossil to modern variance of the distribution of the annual cycle amplitude<sup>35</sup>, a proxy for NINO1+2  
268 interannual variance. Results are not sensitive to the filter type or exact metric (Supplementary  
269 Information). AC amplitude was quantified as the range (maximum minus minimum) of a monthly-  
270 mean seasonal cycle evaluated over each record's time span after high-pass filtering the data with a  
271 10-year smoothing spline<sup>50,51</sup> to avoid the biasing effect of trends. Changes in this quantity were,  
272 likewise, computed as a ratio between fossil and modern samples.

273 Uncertainties in both quantities were estimated via a block-bootstrap procedure<sup>52,53</sup> with  
274 1,000 draws. For interannual variance, the block length was set at 2 years, while for seasonal  
275 amplitude the block length was set to the number of samples per year. Both choices reflect a  
276 compromise between the approximate decorrelation time of the records and the shortness of some  
277 proxy records. For peruvian mollusks, uncertainties were estimated via Monte Carlo simulations  
278 as described in ref 54. The procedure is similar to a block-bootstrap analysis with 5000 draws

279 and block lengths of 1 year using an instrumental time series sampled and disturbed by simulated  
280 proxy-related noises.

281 **Forward modeling of marine bicarbonates.** Although  $\delta^{18}\text{O}$  in marine bicarbonates predom-  
282 inantly reflects either SST<sup>55-57</sup> or seawater  $\delta^{18}\text{O}$  variations resulting from net surface freshwater  
283 balance<sup>58,59</sup>, most corals and mollusks are affected by both variables. This problem may be directly  
284 addressed by explicitly modeling the relationship between the environmental variables and the ob-  
285 served  $\delta^{18}\text{O}$  (i.e. forward modeling<sup>40,60</sup>). Unlike empirical calibration, forward models do not  
286 require assumptions to be made about linearity, the independence of predictors, or the normality  
287 of residuals.

288 A reasonably complete model of the incorporation of  $^{18}\text{O}$  in coral aragonite requires infor-  
289 mation on local ocean temperature, seawater  $^{18}\text{O}$ , pH, insolation and nutrients. However, ref 39  
290 developed a simple bivariate model to predict the  $^{18}\text{O}$  of coral aragonite using SST and SSS as sole  
291 inputs. SSS acts as a proxy for seawater  $^{18}\text{O}$ , with a regionally-dependent coefficients calibrated  
292 over the instrumental era. The thermal dependence is set at  $-0.22\text{‰}/^{\circ}\text{C}$ , close to the expected  
293 slope for inorganic equilibrium fractionation<sup>61</sup>. This model has been shown to capture first-order  
294 variations in the hydrological response of coral  $^{18}\text{O}$ <sup>39,62</sup>. There are known limitations to the use of  
295 such a simple model<sup>62-64</sup>. Specifically, it ignores coral biology and non-equilibrium effects, which  
296 are thought to explain some low-frequency trends in corals<sup>65</sup>. Further, the SSS- $^{18}\text{O}_{\text{sw}}$  slope may not  
297 be constant on millennial timescales<sup>66</sup>, and its spatial variations may severely bias the estimation  
298 of paleo-ENSO variability, particularly in the western Pacific<sup>62</sup>. Nevertheless, we use this model

299 to translate climate model outputs into a  $^{18}\text{O}$  signal for comparison with the observations because  
300 very few of the climate models explicitly simulate water isotopes. The same model may be applied  
301 to simulate  $\delta^{18}\text{O}$  values in the shells of *Tridacna sp* and *Mesodesma donacium*<sup>26,36,37</sup> since they  
302 precipitate aragonite like corals. The slope of the SST- $\delta^{18}\text{O}$  relationship generally used for arago-  
303 nitic mollusks ranges from  $-0.21$  to  $-0.27\text{‰}/^{\circ}\text{C}$ <sup>67,68</sup>, compatible with the slope of  $-0.22\text{‰}/^{\circ}\text{C}$   
304 used by ref 39.

305 We note that recent studies have attempted to quantify uncertainties in inferring changes  
306 in ENSO variance from calibrated proxy observations<sup>42,69</sup>. By using a process model, we es-  
307 chew some of the difficulties associated with calibration, but this passes the uncertainties on to  
308 the process model. Additionally, ref 69 neglected sampling uncertainties, which are central to our  
309 analysis. The existence of non-climatic noise is a problem in every paleoclimate dataset, and the  
310 reader is referred to the original studies for an appraisal of the strength of each climate signal.

311 **Climate Models and Simulations.** We consider the simulations that have been run as part of the  
312 fifth phase of the Coupled Modeling Intercomparison Project (CMIP5)<sup>70</sup> and analyzed in the third  
313 phase of the Palaeoclimate Modelling Intercomparison Project (PMIP3)<sup>27</sup>. This set of simulations  
314 is usually referred to as the CMIP5/PMIP3 experiments, although here we simply refer to them as  
315 PMIP3 experiments. The models used (Supplementary Table 2) are state-of-the-art coupled ocean  
316 atmosphere general circulation models (GCMs), or Earth system models (ESMs) with different  
317 levels of complexity in the forcing used or in the interactions between climate and the carbon  
318 cycle<sup>71</sup>. We consider three experimental designs, following PMIP3 nomenclature:

319 **piControl**

320 The reference are pre-industrial simulations for which Earth's orbit and solar con-  
321 stant are representative of modern conditions, and trace gases, land use and aerosols  
322 are prescribed to AD 1850. The prescribed values vary slightly from one model  
323 to the other. Details are given in [https://wiki.lsce.ipsl.fr/pmip3/  
324 doku.php/pmip3:design:pi:final](https://wiki.lsce.ipsl.fr/pmip3/doku.php/pmip3:design:pi:final).

325 **midHolocene**

326 For the mid-Holocene we use simulations in which Earth orbital parameters and  
327 trace gases have been prescribed to those valid for 6ka<sup>27</sup>. In all the simulations the  
328 date of the vernal equinox is fixed to March 21 at noon. The insolation forcing at  
329 the equator is displayed in Supplementary Figure 9 (see also ref 72, Fig. 3). Details  
330 are given in [https://wiki.lsce.ipsl.fr/pmip3/  
331 design:6k:final](https://wiki.lsce.ipsl.fr/pmip3/doku.php/pmip3:design:6k:final).

332 **Historical**

333 To test the impact of the reference period on the analyses of the simulated change  
334 in the different climates we also consider historical simulations<sup>70</sup> forced with time  
335 evolution of trace gases, volcanic forcing and land-use over the period 1860-2005.  
336 We sampled from the full ensemble of HIST simulations, including several runs  
337 with slightly different initial conditions for each model. In general, their ENSO  
338 statistics were indistinguishable from PI within uncertainties.

339 **Analysis of GCM simulations.** GCM-simulated SST and SSS were translated to  $\delta^{18}\text{O}$  values via  
340 a forward model<sup>39</sup>. Pseudocoral averages over the three main regions (WP, CP, EP) were then  
341 resampled using the above-mentioned block-bootstrap procedure with  $N = 1,000$  draws, before  
342 being subsampled on contiguous 50-year blocks to emulate short observational windows (Supple-  
343 mentary Information, Supplementary Figures S13-S22). We then computed ENSO variance and  
344 AC amplitude, as well as their ratios, for each ensemble member. Probability distributions from  
345 these 1,000 member ensembles were then obtained via kernel density estimation with a bandwidth  
346  $h = 0.15$  (Figure 2).

347 **Regression Analysis.** We use total least squares (TLS) regression (a form of error-in-variables  
348 modeling, closely connected to orthogonal regression<sup>73</sup>), to account for uncertainties in the ENSO -  
349 AC amplitude relationship. TLS steepens regression slopes by taking the potentially biasing effects  
350 of observational noise into account<sup>74</sup>. ENSO variance and AC amplitude ratios were scaled by  
351 their uncertainty (measured by the interquartile range of their block-bootstrap distributions) prior  
352 to TLS regression, to ensure homogenous error magnitudes on both axes of Figure 3. Uncertainties  
353 in regression parameters are estimated via a bootstrap approach<sup>75</sup>, with 2,000 draws.

354 **Wavelet Analysis.** The relationship between ENSO and the AC is also probed via Morlet wavelet  
355 analysis<sup>76</sup>. We sum the energies corresponding to the 2-7y and 0.8-1.2 y bands and report lin-  
356 ear correlations between the resulting series<sup>19</sup>. We do so for all seasonally-resolved, continuous  
357 records in the database (i.e. all except those of refs 26 and 6) and for the PMIP3 *piControl* and  
358 *midHolocene* model outputs, separately for each of the three geographic regions. Statistical signif-

359 icance is established via a non-parametric, isospectral test<sup>77</sup>, which accounts for the loss of degrees  
360 of freedom imparted by smoothing by low-frequency wavelets.

361 **Data.** Data for the paleo observations and model output for the 3 boxes outlined in Fig. 1,  
362 is available via ([https://github.com/CommonClimate/EmileGeay\\_NatGeo2015](https://github.com/CommonClimate/EmileGeay_NatGeo2015)).  
363 The original model data was obtained via the CMIP5/PMIP3 (<http://cmip-pcmdi.llnl.gov/cmip5/>) web site, while the published paleo data were obtained from the National Climatic  
364 Data Center ([https://www.ncdc.noaa.gov/data-access/paleoclimatology-](https://www.ncdc.noaa.gov/data-access/paleoclimatology-data)  
365 [data](https://www.ncdc.noaa.gov/data-access/paleoclimatology-data)).  
366

367 **Code Availability.** Matlab/Python code to reproduce the block bootstrap, wavelet and re-  
368 gression analysis is available at [https://github.com/CommonClimate/EmileGeay\\_](https://github.com/CommonClimate/EmileGeay_NatGeo2015)  
369 [NatGeo2015](https://github.com/CommonClimate/EmileGeay_NatGeo2015). In particular, these codes generate the probability distributions for all the ratios  
370 plotted in Fig. 2, except those associated with ref 26. The Matlab code to generate the latter distri-  
371 butions is available at [http://www.isem.univ-montp2.fr/carre\\_matthieu](http://www.isem.univ-montp2.fr/carre_matthieu), using  
372 the parameter values published in ref 54 (SOM).

## Bibliography

1. Sarachik, E. S. & Cane, M. A. *The El Niño-Southern Oscillation Phenomenon*. 336 pages (Cambridge University Press, Cambridge, UK, 2010).
2. Collins, M. *et al.* The impact of global warming on the tropical Pacific Ocean and El Niño. *Nature Geosci* **3**, 391–397 (2010).
3. Schmidt, G. A. Enhancing the relevance of palaeoclimate model/data comparisons for assessments of future climate change. *Journal of Quaternary Science* **25**, 79–87 (2010).
4. Braconnot, P., Luan, Y., Brewer, S. & Zheng, W. Impact of Earth's orbit and freshwater fluxes on Holocene climate mean seasonal cycle and ENSO characteristics. *Climate Dynamics* **38**, 1081–1092 (2012).
5. Tudhope, A. W. *et al.* Variability in the El Niño-Southern Oscillation through a glacial-interglacial cycle. *Science* **291**, 1511–1517 (2001).
6. McGregor, H. V. & Gagan, M. K. Western Pacific coral  $\delta^{18}\text{O}$  records of anomalous Holocene variability in the El Niño-Southern Oscillation. *Geophysical Research Letters* **31** (2004).
7. Koutavas, A. & Joannides, S. El Niño-Southern Oscillation extrema in the Holocene and Last Glacial Maximum. *Paleoceanography* **27**, PA4208 (2012).
8. Clement, A. C., Seager, R. & Cane, M. A. Suppression of El Niño during the mid-Holocene by changes in the Earth's orbit. *Paleoceanography* **15**, 731–737 (2000).

- 392 9. Liu, Z., Kutzbach, J. & Wu, L. Modeling climate shift of El Niño variability in the Holocene.  
393 *Geophysical Research Letters* **27**, 2265–2268 (2000).
- 394 10. Zheng, W., Braconnot, P., Guilyardi, E., Merkel, U. & Yu, Y. ENSO at 6ka and 21ka from  
395 ocean–atmosphere coupled model simulations. *Clim. Dyn.* **30**, 745–762 (2008).
- 396 11. Chiang, J. C. H., Fang, Y. & Chang, P. Pacific Climate Change and ENSO Activity in the  
397 Mid-Holocene. *Journal of Climate* **22**, 923–939 (2009).
- 398 12. An, S.-I. & Choi, J. Mid-Holocene tropical Pacific climate state, annual cycle, and ENSO in  
399 PMIP2 and PMIP3. *Climate Dynamics* **43**, 957–970 (2014).
- 400 13. Liu, Z. *et al.* Evolution and forcing mechanisms of El Niño over the past 21,000 years. *Nature*  
401 **515**, 550–553 (2014).
- 402 14. Wang, X. L. The coupling of the annual cycle and ENSO over the tropical Pacific. *Journal of*  
403 *the Atmospheric Sciences* **51**, 1115–1136 (1994).
- 404 15. Chang, P., Wang, B., Li, T. & Ji, L. Interactions between the seasonal cycle and the Southern  
405 Oscillation - Frequency entrainment and chaos in a coupled ocean-atmosphere model. *Geo-*  
406 *phys. Res. Lett.* **21**, 2817–2820 (1994).
- 407 16. Guilyardi, E. El Niño mean state seasonal cycle interactions in a multi-model ensemble. *Clim.*  
408 *Dyn.* **26**, 329–348 (2006).

- 409 17. Timmermann, A., Lorenz, S. J., An, S.-I., Clement, A. & Xie, S.-P. The effect of orbital  
410 forcing on the mean climate and variability of the tropical pacific. *Journal of Climate* **20**,  
411 4147–4159 (2007).
- 412 18. An, S.-I. *et al.* The inverse effect of annual-mean state and annual-cycle changes on ENSO.  
413 *Journal of Climate* **23**, 1095–1110 (2010).
- 414 19. An, S.-I. & Choi, J. Inverse relationship between the equatorial eastern Pacific annual-cycle  
415 and ENSO amplitudes in a coupled general circulation model. *Climate Dynamics* **40**, 663–675  
416 (2013).
- 417 20. Liu, Z. A simple model study of ENSO suppression by external periodic forcing. *J. Clim.* **15**,  
418 1088–1098 (2002).
- 419 21. Tziperman, E., Stone, L., Cane, M. A. & Jarosh, H. El Niño chaos: overlapping of resonances  
420 between the seasonal cycle and the Pacific ocean-atmosphere oscillator. *Science* **264**, 72–74  
421 (1994).
- 422 22. Jin, F.-F., Neelin, J. D. & Ghil, M. El Niño on the Devil’s staircase: annual subharmonic steps  
423 to chaos. *Science* **264**, 70–72 (1994).
- 424 23. Stuecker, M. F., Timmermann, A., Jin, F.-F., McGregor, S. & Ren, H.-L. A combination mode  
425 of the annual cycle and the El Niño-Southern Oscillation. *Nature Geosci* **6**, 540–544 (2013).
- 426 24. McGregor, H. V. *et al.* A weak El Niño-Southern Oscillation with delayed seasonal growth  
427 around 4,300 years ago. *Nature Geoscience* **6**, 949–953 (2013).

- 428 25. Cobb, K. M. *et al.* Highly variable El Niño-Southern Oscillation throughout the Holocene.  
429 *Science* **339**, 67–70 (2013).
- 430 26. Carré, M. *et al.* Holocene history of ENSO variance and asymmetry in the eastern tropical  
431 Pacific. *Science* **345**, 1045–1048 (2014).
- 432 27. Braconnot, P. *et al.* Evaluation of climate models using palaeoclimatic data. *Nature Clim.*  
433 *Change* **2**, 417–424 (2012).
- 434 28. Cobb, K. M., Charles, C. D., Cheng, H. & Edwards, R. L. El Niño/Southern Oscillation and  
435 tropical Pacific climate during the last millennium. *Nature* **424**, 271–276 (2003).
- 436 29. Duprey, N. *et al.* Early mid-Holocene SST variability and surface-ocean water balance in the  
437 southwest Pacific. *Paleoceanography* **27**, PA4207 (2012).
- 438 30. Kilbourne, K. H., Quinn, T. M., Taylor, F. W., Delcroix, T. & Gouriou, Y. El Niño-Southern  
439 Oscillation-related salinity variations recorded in the skeletal geochemistry of a *Porites* coral  
440 from Espiritu Santo, Vanuatu. *Paleoceanography* **19**, PA4002 (2004).
- 441 31. Woodroffe, C. D. & Gagan, M. K. Coral microatolls from the central Pacific record Late  
442 Holocene El Niño. *Geophysical Research Letters* **27**, 1511–1514 (2000).
- 443 32. Woodroffe, C. D., Beech, M. R. & Gagan, M. K. Mid-late Holocene El Niño variability in the  
444 equatorial Pacific from coral microatolls. *Geophysical Research Letters* **30**, 1358 (2003).
- 445 33. Evans, M., Fairbanks, R. & Rubenstone, J. A proxy index of ENSO teleconnections. *Nature*  
446 **394**, 732–733 (1998).

- 447 34. McGregor, H. V., Fischer, M. J., Gagan, M. K., Fink, D. & Woodroffe, C. D. Environmen-  
448 tal control of the oxygen isotope composition of *Porites* coral microatolls. *Geochimica et*  
449 *Cosmochimica Acta* **75**, 3930–3944 (2011).
- 450 35. Carré, M., Sachs, J. P., Schauer, A. J., Rodríguez, W. E. & Ramos, F. C. Reconstructing El  
451 Niño-Southern Oscillation activity and ocean temperature seasonality from short-lived marine  
452 mollusk shells from Peru. *Palaeogeography, Palaeoclimatology, Palaeoecology* **371**, 45–53  
453 (2013).
- 454 36. Driscoll, R. *et al.* ENSO Reconstructions over the past 60 ka using giant clams (*Tridacna* sp.)  
455 from Papua New Guinea. *Geophysical Research Letters* **41**, 6819–6825 (2014).
- 456 37. Welsh, K., Elliot, M., Tudhope, A., Ayling, B. & Chappell, J. Giant bivalves (*Tridacna gigas*)  
457 as recorders of ENSO variability. *Earth and Planetary Science Letters* **307**, 266–270 (2011).
- 458 38. McGregor, S., Timmermann, A., England, M. H., Elison Timm, O. & Wittenberg, A. T. In-  
459 ferred changes in El Niño-Southern Oscillation variance over the past six centuries. *Climate*  
460 *of the Past* **9**, 2269–2284 (2013).
- 461 39. Thompson, D. M., Ault, T. R., Evans, M. N., Cole, J. E. & Emile-Geay, J. Comparison of  
462 observed and simulated tropical climate trends using a forward model of coral  $\delta^{18}\text{O}$ . *Geophys.*  
463 *Res. Lett.* **38**, L14706 (2011).
- 464 40. Dee, S. G. *et al.* PRYSM: an open-source framework for proxy system modeling, with appli-  
465 cations to oxygen-isotope systems. *J. Adv. Mod. Earth Sys.* **07** (2015).

- 466 41. Wittenberg, A. T. Are historical records sufficient to constrain ENSO simulations? *Geophys.*  
467 *Res. Lett.* **36**, L12702 (2009).
- 468 42. Russon, T., Tudhope, A. W., Hegerl, G. C., Schurer, A. & Collins, M. Assessing the signif-  
469 icance of changes in ENSO amplitude using variance metrics. *Journal of Climate* **27**, 4911–  
470 4922 (2014).
- 471 43. Kug, J.-S., Jin, F.-F. & An, S.-I. Two types of El Niño events: Cold tongue El Niño and warm  
472 pool El Niño. *Journal of Climate* **22**, 1499–1515 (2009).
- 473 44. Karamperidou, C., Di Nezio, P. N., Timmermann, A., Jin, F.-F. & Cobb, K. M. The response of  
474 ENSO flavors to mid-Holocene climate: Implications for proxy interpretation. *Paleoceanog-*  
475 *raphy* **30**, 527–547 (2015).
- 476 45. Newman, M., Shin, S.-I. & Alexander, M. A. Natural variation in ENSO flavors. *Geophys.*  
477 *Res. Lett.* **38** (2011).
- 478 46. Luan, Y., Braconnot, P., Yu, Y. & Zheng, W. Tropical Pacific mean state and ENSO changes:  
479 sensitivity to freshwater flux and remnant ice sheets at 9.5 ka BP. *Climate Dynamics* **44**,  
480 661–678 (2015).
- 481 47. Roberts, W. H. G., Battisti, D. S. & Tudhope, A. W. ENSO in the mid-Holocene according to  
482 CSM and HadCM3. *Journal of Climate* **27**, 1223–1242 (2013).
- 483 48. Bellenger, H., Guilyardi, E., Leloup, J., Lengaigne, M. & Vialard, J. ENSO representation in  
484 climate models: from CMIP3 to CMIP5. *Climate Dynamics* **42**, 1999–2018 (2014).

- 485 49. Lloyd, J., Guilyardi, E. & Weller, H. The Role of Atmosphere Feedbacks during ENSO in the  
486 CMIP3 Models. Part III: The Shortwave Flux Feedback. *Journal of Climate* **25**, 4275–4293  
487 (2012).
- 488 50. Cook, E. R. & Peters, K. The smoothing spline: A new approach to standardizing forest  
489 interior tree-ring width series for dendroclimatic studies. *Tree-Ring Bulletin* **41**, 45–53 (1981).
- 490 51. Weinert, H. L. A fast compact algorithm for cubic spline smoothing. *Computational Statistics*  
491 *& Data Analysis* **53**, 932–940 (2009).
- 492 52. Efron, B. & Tibshirani, R. J. *An Introduction to the Bootstrap* (Chapman & Hall, New York,  
493 1993).
- 494 53. Kunsch, H. R. The jackknife and the bootstrap for general stationary observations. *The Annals*  
495 *of Statistics* **17**, 1217–1241 (1989).
- 496 54. Carré, M., Sachs, J. P., Wallace, J. M. & Favier, C. Exploring errors in paleoclimate proxy  
497 reconstructions using monte carlo simulations: paleotemperature from mollusk and coral geo-  
498 chemistry. *Climate of the Past* **8**, 433–450 (2012).
- 499 55. Dunbar, R. B., Wellington, G. M., Colgan, M. W. & Glynn, P. W. Eastern Pacific sea sur-  
500 face temperature since 1600 A.D.: The  $\delta^{18}\text{O}$  record or climate variability in Galápagos corals.  
501 *Paleoceanography* **9**, 291–316 (1994).
- 502 56. Evans, M., Fairbanks, R. & Rubenstone, J. The thermal oceanographic signal of  
503 El Niño reconstructed from a Kiritimati Island coral. *Journal of Geophysical Research*  
504 (*Oceans*) **104**, 13409–13422 (1999).

- 505 57. Cobb, K. M., Charles, C. D. & Hunter, D. E. A central tropical Pacific coral demonstrates  
506 Pacific, Indian, and Atlantic decadal climate connections. *Geophys. Res. Lett.* **28**, 2209–2212  
507 (2001).
- 508 58. Fairbanks, R. G. *et al.* Evaluating climate indices and their geochemical proxies measured in  
509 corals. *Coral Reefs* **16**, S93–S100 (1997).
- 510 59. Conroy, J. L., Cobb, K. M., Lynch-Stieglitz, J. & Polissar, P. J. Constraints on the salinity–  
511 oxygen isotope relationship in the central tropical pacific ocean. *Marine Chemistry* **161**, 26–33  
512 (2014).
- 513 60. Evans, M. N., Tolwinski-Ward, S. E., Thompson, D. M. & Anchukaitis, K. J. Applications of  
514 proxy system modeling in high resolution paleoclimatology. *Quaternary Science Reviews* **76**,  
515 16–28 (2013).
- 516 61. McConnaughey, T.  $^{13}\text{C}$  and  $^{18}\text{O}$  isotopic disequilibrium in biological carbonates: I. Patterns.  
517 *Geochim. Cosmochim. Acta.* **53**, 151–162 (1989).
- 518 62. Russon, T., Tudhope, A. W., Hegerl, G. C., Collins, M. & Tindall, J. Inter-annual tropical  
519 Pacific climate variability in an isotope-enabled CGCM: implications for interpreting coral  
520 stable oxygen isotope records of ENSO. *Climate of the Past* **9**, 1543–1557 (2013).
- 521 63. Stevenson, S., McGregor, H. V., Phipps, S. J. & Fox-Kemper, B. Quantifying errors in coral-  
522 based ENSO estimates: Toward improved forward modeling of  $\delta^{18}\text{O}$ . *Paleoceanography* **28**,  
523 633–649 (2013).

- 524 64. Thompson, D. M. *et al.* Coral-model comparison highlighting the role of salinity in long-term  
525 trends. *PAGES Newsletter* **21**, 60–61 (2013).
- 526 65. Lough, J. A strategy to improve the contribution of coral data to high-resolution paleoclima-  
527 tology. *Palaeogeography, Palaeoclimatology, Palaeoecology* **204**, 115 – 143 (2004).
- 528 66. LeGrande, A. N. & Schmidt, G. A. Water isotopologues as a quantitative paleosalinity proxy.  
529 *Paleoceanography* **26**, PA3225 (2011).
- 530 67. Grossman, E. L. & Ku, T.-L. Oxygen and carbon isotope fractionation in biogenic aragonite:  
531 Temperature effects. *Chemical Geology: Isotope Geoscience section* **59**, 59–74 (1986).
- 532 68. Carré, M. *et al.* Stable isotopes and sclerochronology of the bivalve *Mesodesma donacium*: Po-  
533 tential application to Peruvian paleoceanographic reconstructions. *Palaeogeography, Palaeo-*  
534 *climatology, Palaeoecology* **228**, 4–25 (2005).
- 535 69. Russon, T., Tudhope, A. W., Collins, M. & Hegerl, G. C. Inferring changes in ENSO amplitude  
536 from the variance of proxy records. *Geophysical Research Letters* 2014GL062331 (2015).
- 537 70. Taylor, K. E., Stouffer, R. J. & Meehl, G. A. An overview of CMIP5 and the experiment  
538 design. *Bulletin of the American Meteorological Society* **93**, 485–498 (2011).
- 539 71. Flato, G. *et al.* Evaluation of Climate Models. In Stocker, T. F. *et al.* (eds.) *Climate Change*  
540 *2013: The Physical Science Basis. Contribution of Working Group I to the Fifth Assessment*  
541 *Report of the Intergovernmental Panel on Climate Change*, 741–866 (Cambridge University  
542 Press, Cambridge, United Kingdom and New York, NY, USA, 2013).

- 543 72. Luan, Y., Braconnot, P., Yu, Y., Zheng, W. & Marti, O. Early and mid-Holocene climate in  
544 the tropical Pacific: seasonal cycle and interannual variability induced by insolation changes.  
545 *Climate of the Past* **8**, 1093–1108 (2012).
- 546 73. Van Huffel, S. *Total least squares and errors-in-variables modeling: bridging the gap between*  
547 *statistics, computational mathematics and engineering*, 539–555 (Physica-Verlag HD, 2004).
- 548 74. Markovsky, I., Sima, D. M. & Van Huffel, S. Total least squares methods. *Wiley Interdisci-*  
549 *plinary Reviews: Computational Statistics* **2**, 212–217 (2010).
- 550 75. Pešta, M. Total least squares and bootstrapping with applications in calibration. *Statistics* **47**,  
551 966–991 (2013).
- 552 76. Torrence, C. & Compo, G. P. A practical guide to wavelet analysis. *Bull. Amer. Meteor. Soc.*  
553 **79**, 61–78 (1998).
- 554 77. Ebisuzaki, W. A method to estimate the statistical significance of a correlation when the data  
555 are serially correlated. *Journal of Climate* **10**, 2147–2153 (1997).

556 **Supplementary Information** is linked to the online version of the paper at [www.nature.com/ngeo](http://www.nature.com/ngeo).  
557 [www.nature.com/ngeo](http://www.nature.com/ngeo).

## 558 **Acknowledgements**

559 We thank the referees for constructive reviews that improved the manuscript. All data, metadata  
560 and code [will be] archived at [zenodo.org](http://zenodo.org). We acknowledge the World Climate Research Pro-

561 gram's Working Group on Coupled Modelling, which is responsible for CMIP, and we thank the  
562 PMIP3 modeling groups for producing and making available their model output. The U.S. Depart-  
563 ment of Energy's Program for Climate Model Diagnosis and Intercomparison provides coordinat-  
564 ing support for CMIP, and led development of software infrastructure in partnership with the Global  
565 Organization for Earth System Science Portals. JEG acknowledges support from US NSF grant  
566 DMS 1025465. KMC acknowledges support from NOAA award NA11OAR4310166 and NSF  
567 award OCE-0752091. M. Collins acknowledges support from UK NERC grant NE/H009957/1.  
568 HVM and AT acknowledge support from Australian Research Council (ARC) Discovery Project  
569 grant DP1092945. HVM is supported by an ARC Future Fellowship FT140100286 grant. AT  
570 acknowledges support from UK NERC grant NE/H009957/1. TC thanks M. McCulloch (formerly  
571 at ANU) for dating the Bayes coral, and M. Gagan's team at ANU for help with isotopic mea-  
572 surements. The Bayes 1 core was collected with funds from the Institut de Recherche pour le  
573 Développement. BS was supported by the DFG Cluster of Excellence "The Future Ocean" (EXC  
574 80/2). PB, M. Carré, TC, JL, ME and AT were supported by the French National Research Agency  
575 under EL PASO grant (no. 2010 298 BLANC 608 01). This project also serves for coordina-  
576 tion and implementation of the PMIP3/CMIP5 simulations on the ESGF distributed database. We  
577 thank Jean-Yves Peterschmitt for his help with the PMIP database. This work was initiated in a  
578 workshop co-sponsored by WCRP/CLIVAR, IGBP/PAGES, INQUA, and IPSL in 2011.

579 **Author Contributions**

580 J.E.G. designed the study, performed the analysis, lead the writing, and prepared the manuscript.  
581 P.B. coordinated the synthesis. M.Carré, K.M.C, T.C., M.E. and R.D. contributed data and/or  
582 analysis. P.B. and J.L. analyzed simulations and contributed to writing. Y.Z. processed PMIP3  
583 output and generated some of the supplementary figures. A.T., B.S., M.Collins provided input in  
584 the analysis and interpretation. J.E.G., K.M.C., M.Carré, S.P.H., H.V.M., T.C., P.B. and A.T. wrote  
585 the paper. All authors reviewed the manuscript.

586 **Author information**

587 Reprints and permissions information is available at [www.nature.com/reprints](http://www.nature.com/reprints). The au-  
588 thors declare no competing financial interests. Correspondence and requests for materials should  
589 be addressed to [julieneg@usc.edu](mailto:julieneg@usc.edu).

590 **Figure 1** Location and ENSO sensitivity of proxy archives. Circles denote corals, stars  
591 denote mollusks. Contours denote biocarbonate  $\delta^{18}\text{O}$  composites ( $\text{‰}$  per  $^{\circ}\text{C}$  of NINO3.4  
592 SST) derived from the model of Thompson et al.<sup>39</sup> driven by NCEP OI analysis v2 SST  
593 and SODA 2.2.4 SSS over 1981-2010 boreal winters (Supplementary Figures S8-S9).  
594  $\delta^{18}\text{O}$  values were regressed onto NINO3.4 SST to highlight relationships to ENSO. The  
595 three equatorial study regions (West, Center & East) are delineated by boxes. Note that  
596 refs. 11,12,15,16,18-21 all use data from Kiritimati ( $1^{\circ}53'\text{N},157^{\circ}24'\text{W}$ ).

597 **Figure 2** (top) Changes in ENSO variance and AC amplitude over the Holocene. LEFT  
598 column: Changes in ENSO-band (2-7y) variance between fossil and modern samples  
599 in the West (top), Center (middle) and East (bottom). Horizontal bars mark the period  
600 covered by each dataset; except for mollusks from the Peruvian coast, these are nar-  
601 rower than the symbol width. Ellipses represent uncertainties about these ratios in both  
602 dimensions: the width represents a 95% CI for the central date of each sample, based  
603 on reported analytical uncertainty on radiometric ages; the vertical component is a 95%  
604 CI for the variance ratio, obtained via a block-bootstrap procedure (Methods). Unity (no  
605 change) is marked by a dashed gray line. Similar statistics derived from PMIP3 models on  
606 50-year windows are depicted on side panels for *piControl* and *midHolocene* experiments.  
607 Solid lines are kernel density estimates of those distributions (Methods), while dashed  
608 lines indicate their median. RIGHT column: idem for AC amplitude.

		Quantiles		
Period	Region	2.5%	50%	97.5%
[h] 5.5 – 7.5 kyBP	West	-125%	50%	92%
	Center	-5%	66%	92%
	East	-16%	33%	69%
3–5 kyBP	West	-54%	35%	61%
	Center	28%	64%	84%
	East	-18%	58%	109%

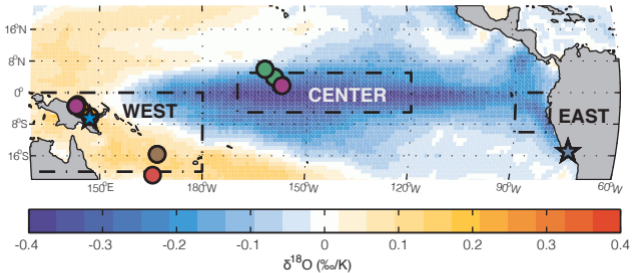
Table 1: Observed reductions in ENSO variance in the tropical Pacific during the MH (5.5–7.5 kyBP) and the 3-5 kyBP interval. The numbers represent quantiles of the block-bootstrap ensembles. By convention, a negative reduction implies an increase.

$H_0$	HadGEM2	GISS	KCM	CCSM4	MIROC	MPI	CNRM	IPSL	CSIRO
[h] PI null	1.37%	11.98%	1.62%	3.66%	2.82%	3.55%	0.88%	2.06%	5.00%
MH null	3.12%	3.16%	3.35%	5.60%	7.36%	9.78%	3.81%	15.50%	0.21%

Table 2: Probability of observing periods of reduced ENSO activity in the CP in nine GCMs. Top row: frequency of occurrence of 50-year long periods for which the ENSO variance ratio is as low as the 3-5 kyBP average inferred from paleoclimate observations (0.36 – a 64% reduction) in pre-industrial (*piControl*) simulations. Bottom row: same for *midHolocene* simulations

609 **Figure 3** (top) Link between ENSO variance and the seasonal cycle in proxy obser-  
610 vations (top) and PMIP3 models (bottom). The observed values are for all seasonally-  
611 resolved records from the Pacific during the whole of the past 10 ky. The simulated values  
612 are based on 50-year segments from the *midHolocene* and *piControl* simulations. On top,  
613 symbology as in Figure 1. On the bottom, triangles denote the median of *piControl* simula-  
614 tions, squares the median of *midHolocene* simulations. Data from the eastern, central and  
615 western Pacific were pooled together, scaled by their interquartile range so their uncer-  
616 tainties on both axes are commensurate. An orthogonal regression (total least squares)  
617 fit is presented for both datasets, together with approximate 95% CIs (dashed lines) and  
618 probability density (gray contours) obtained via bootstrap resampling (Methods).

# Proxy locations & El Niño composite $\delta^{18}\text{O}$



● ref. 29, 30

● this study

● ref. 25, 28

● ref. 31, 32

● ref. 6, 24, 30-34

● ref. 5

★ ref. 26, 35

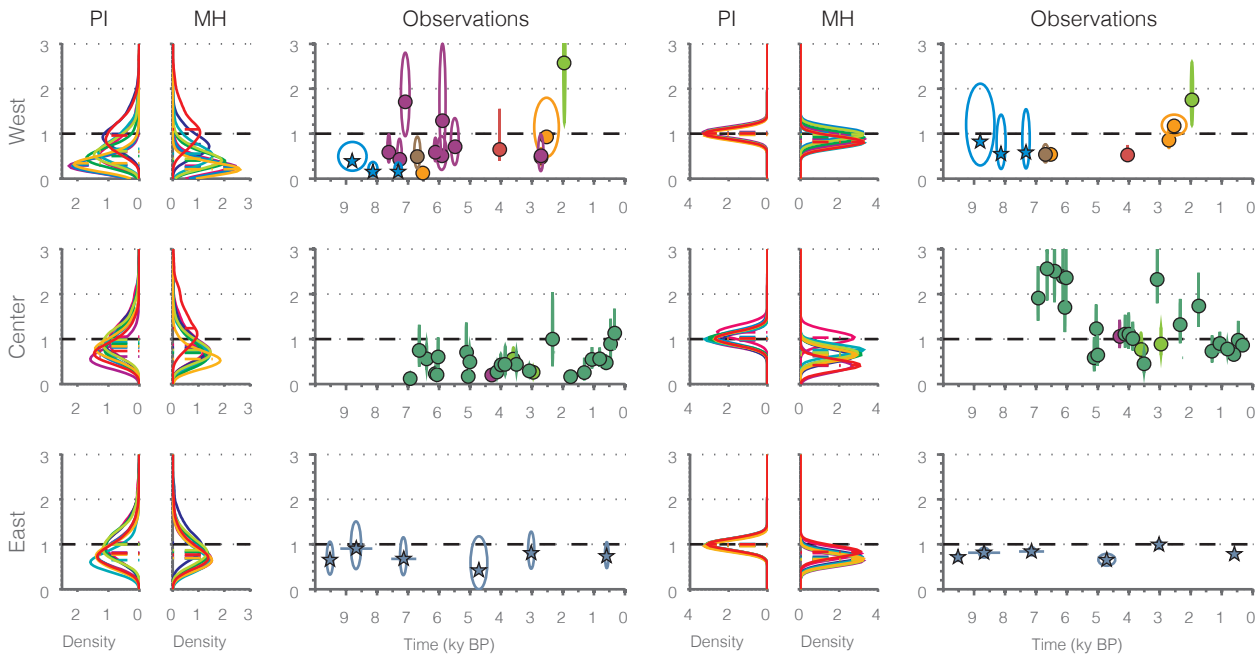
★ ref. 36, 37

○ Coral

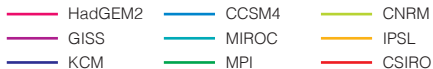
★ Mollusk

## ENSO variance ratio

## AC amplitude ratio



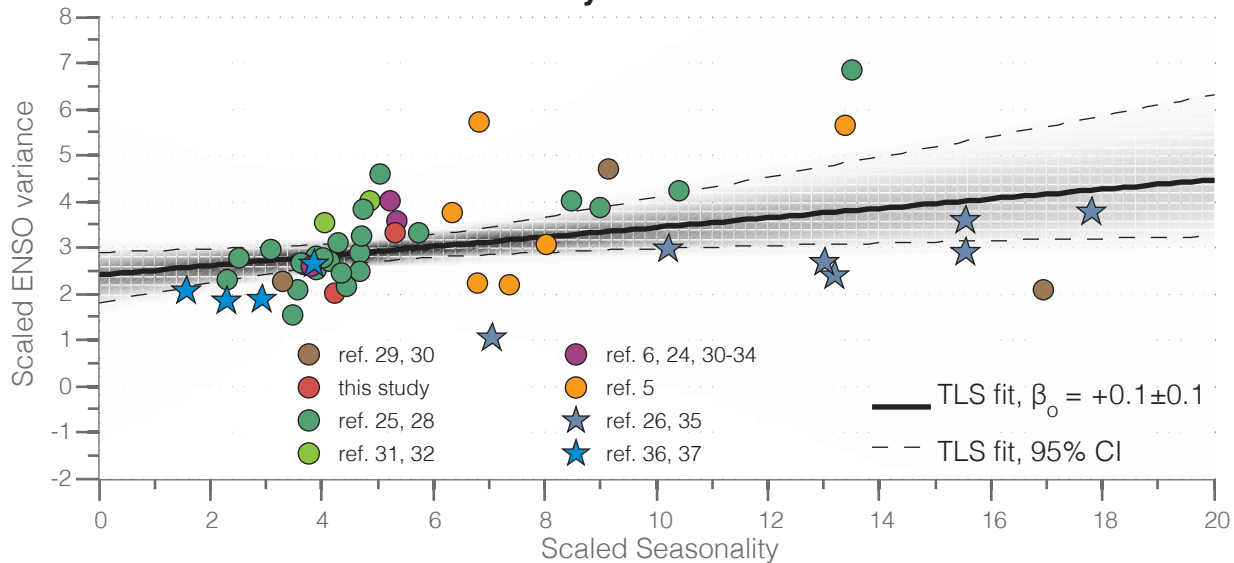
### GCMs



### Observations



## Proxy Observations



## General Circulation Models

